

UNCLASSIFIED

Defense Technical Information Center  
Compilation Part Notice

ADP023755

TITLE: Spatial Processing of Urban Acoustic Wave Fields from  
High-Performance Computations

DISTRIBUTION: Approved for public release, distribution unlimited

This paper is part of the following report:

TITLE: Proceedings of the HPCMP Users Group Conference 2007. High  
Performance Computing Modernization Program: A Bridge to Future  
Defense held 18-21 June 2007 in Pittsburgh, Pennsylvania

To order the complete compilation report, use: ADA488707

The component part is provided here to allow users access to individually authored sections  
of proceedings, annals, symposia, etc. However, the component should be considered within  
the context of the overall compilation report and not as a stand-alone technical report.

The following component part numbers comprise the compilation report:

ADP023728 thru ADP023803

UNCLASSIFIED

# Spatial Processing of Urban Acoustic Wave Fields from High-Performance Computations

Stephen A. Ketcham, D. Keith Wilson, Harley H. Cudney, and Michael W. Parker  
USACE Engineer Research and Development Center, Cold Regions Research and Engineering  
Laboratory (ERDC-CRREL), Hanover, NH

{Stephen.A.Ketcham, D.Keith.Wilson, Harley.H.Cudney, Michael.W.Parker}@erdc.usace.army.mil

## Abstract

*Future US Army ground sensors in urban terrain will process acoustic signals to detect, classify, and locate sources of interest. Optimal processing will require understanding of the effects of the urban infrastructure on sound propagation. These include multi-path phenomena that will complicate sensing, and must be accounted for in sensor placement and performance algorithms. The objective of this work is to develop spatial processing techniques for acoustic wave propagation data from three-dimensional high-performance computations to quantify scattering due to urban structures and develop reduced-order models of wave-field data. The work applies Fourier analysis to urban acoustic wave-field data to generate measures of signal fading caused by scattering. The work calculates these measures from ratios of Fourier transforms of wave-field signals with and without scattering to isolate the structure-induced scattering. In addition, we calculate impulse response functions of acoustic wave-field data, and use these functions as the input to a system realization algorithm to produce reduced-order wave-field models. The results include signal fading as functions of distance and frequency for an urban acoustic model that includes structures like those in a small-city periphery. The results also include predicted acoustic wave-field signals from reduced-order models in comparison with full-model signals. We conclude that the spatial processing of urban acoustic wave fields from high-performance computations produces broadly useful measures for understanding and modeling urban wave propagation.*

## 1. Introduction

Future US Army ground sensors operating in urban terrain will rely in part on acoustic components to detect, classify, and locate mortar and sniper fire and other sources of interest. Optimal sensing and processing of

acoustic signals will require understanding of the effects of the urban infrastructure on sound propagation. These include multi-path scattering from multiple reflections that cause energy from a source to arrive at a sensor location from many directions, with phase interference that can severely limit amplitude and coherence of arriving energy. These effects will complicate sensing, and must be accounted for in sensor placement and performance algorithms.

Our objective is to develop spatial processing techniques for acoustic wave propagation data from three-dimensional high-performance computations to (1) quantify scattering due to urban structures and (2) develop reduced-order models to produce wave-field data. The techniques will ultimately support development of decision support tools for sensor placement and performance and reduced-order high fidelity models that account for effects of urban structures on propagation.

The approach we employ to quantify scattering derives from recent work by Wilson, et al.<sup>[1,2]</sup>, who concluded that statistical relationships of signal fading and coherence with distance in urban environments can be parameterized like corresponding functions for wind-turbulence-induced scattering. The practical significance is that the existing US Army decision-support tool SPEBE<sup>[3]</sup>, which accounts for the effect of turbulence on sound propagation by scattering functions, can be updated for use in urban environments with statistical scattering parameters derived for urban acoustics. Wilson, et al.<sup>[1,2]</sup>, based their work on two-dimensional modeling of harmonic sound-wave scattering caused by building-like structures. The current work applies Fourier analysis to multiple three-dimensional urban-acoustic data sets to generate statistical measures of signal fading. Our initial interest is in measures that are independent of particular configurations of urban structures and source locations, so that they can be useful when it is impractical or unnecessary to directly model urban sound propagation. The work calculates fading measures from ratios of Fourier transforms of wave-field signals with and without

scattering—the latter from otherwise-identical models without urban structures—to isolate the structure-induced scattering. Subsequent analyses will focus on signal coherence.

In addition, we calculate frequency response functions of acoustic wave-field data, and use these functions as the input to a system realization algorithm to produce reduced-order wave-field models. Reduced-order models (ROMs) are low-order models derived from a projection of a dynamic system's degrees of freedom to a smaller set that reproduces the system's essential dynamics within a desired error level<sup>[4]</sup>. ROMs can provide quantitatively accurate descriptions at a computational cost much lower than the original numerical model, and a means to readily interpret system dynamics<sup>[4]</sup>. We apply state-space realization theory and singular-value-decomposition (SVD) model-order reduction<sup>[5,6]</sup> to wave-field data. By this approach we begin to look ahead to large-scale high-fidelity models that compute in real time or near-real time for specific urban configurations, yet have the capability to model sound propagation with severe multi-path scattering.

The results include signal-fading functions of distance and frequency from urban acoustic models that include structures like those in a small-city periphery. These show that the sound diminishes exponentially with distance when non-line-of-site locations become dominant in the averaged data, as is the case for turbulent scattering. In addition, the signal fading appears to be independent of frequency for most of the bandwidth of the analyses. These substantiate signal-fading results found previously by Wilson, et al.<sup>[1,2]</sup>. The results also include predicted acoustic wave fields from reduced-order models, in comparison with full-model wave fields. We conclude that the spatial processing of urban acoustic wave fields from high-performance computations produces broadly useful measures for understanding and modeling urban wave propagation.

## 2. Spatial Processing Methodology

We perform acoustic wave propagation analyses using three-dimensional finite-difference time-domain (FDTD) computations. Our spatial processing uses the input and response signals for Fourier analysis. We apply transforms of the sound-pressure wave-field response for both scattering and reduced-order modeling analyses. The former applies ratios of wave-field and reference-model Fourier transforms, and the latter applies the frequency response between a source history and the sound pressure response.

### 2.1. High-Performance Computations

Our FDTD method solves the following first-order partial differential equations for a linear time-invariant acoustic medium References 7 and 8:

$$\frac{\partial p}{\partial t} = -\rho c^2 \left( \frac{\partial v_x}{\partial x} + \frac{\partial v_y}{\partial y} + \frac{\partial v_z}{\partial z} - Q \right) \quad (1)$$

$$\begin{aligned} \frac{\partial v_x}{\partial t} &= -\frac{1}{\rho} \left( \frac{\partial p}{\partial x} + \sigma v_x \right) \\ \frac{\partial v_y}{\partial t} &= -\frac{1}{\rho} \left( \frac{\partial p}{\partial y} + \sigma v_y \right) \\ \frac{\partial v_z}{\partial t} &= -\frac{1}{\rho} \left( \frac{\partial p}{\partial z} + \sigma v_z \right) \end{aligned} \quad (2)$$

where  $p(x, y, z, t)$  is pressure;  $v_x$ ,  $v_y$ , and  $v_z$  are the components of the particle velocity vector  $v(x, y, z, t)$ ;  $\rho$ ,  $c$ , and  $\sigma$  are the material density, speed of sound, and flow resistivity, respectively; and  $Q$  is the dilatation-rate source. The method discretizes the solution domain using second-order finite differences both in time and on a Cartesian variable staggered grid<sup>[9]</sup>, and applies an absorbing boundary condition<sup>[10]</sup> at the model edges. The difference equations allow inhomogeneous material properties  $\rho = \rho(x, y, z)$ ,  $\kappa = \kappa(x, y, z)$ , and  $\sigma = \sigma(x, y, z)$ , and source time series  $Q(t)$  at selected locations  $(x_s, y_s, z_s)$ . We assign nonzero flow resistivity terms only to model porous media, i.e., to model impedance of porous ground and construction materials and the resulting reflections of sound waves in air at air/porous media interfaces.

The propagation models, described in Reference 11, are of the ground and buildings of sub areas of a small-city periphery as defined in an urban template model<sup>[12]</sup>. We focus on external acoustics by using solid blocks for the buildings. Two materials make up the current models: air and a porous material used to model both the ground and buildings. The choice of porous properties produced a strongly reflective high-impedance surface<sup>[8]</sup> at the material interfaces. Figure 1 shows one of nine urban models with results presented herein. Each of the nine contains a different area of the small-city periphery template, with a randomly selected center, for statistical analysis. An additional model, without buildings, produced reference propagation results for scattering analysis. Each of these models had  $x \times y \times z$  dimensions of  $285 \times 285 \times 66$  m using  $2,336 \times 2,328 \times 508$  nodes.

The source location in each model was 1.062 m above the ground surface at  $(x_s, y_s) = (142.8, 142.4)$ , which is at the center of the model  $x, y$  plan view. The source history was a filtered pulse designed to produce responses for broadband Fourier analysis and to minimize high-frequency dispersion errors in the analyses. Figure 2 illustrates (a) the unit-less source time series  $g$  between

$t = 0.1$  and  $0.2$  s, which was scaled by  $Q = 35.4$  (1/s) for input to the analysis, and (b) the broadband energy spectrum of the time series. The model grid spacing is  $0.118$  m, and the speed of sound in the air is  $347$  m/s. At  $300$  Hz, where the source energy is strongly reduced, this translates to approximately 10 nodes per wavelength.

An example snapshot of the propagation is in Figure 3. This figure shows the pressure wave field  $0.6$  m above the ground and building rooftops, which is the  $x, y$  wave field analyzed in subsequent results. The full simulation was  $1.6$  s, which corresponds to a duration that would allow a waveform to spread outward to a radius equal to twice the width of the model. We considered this sufficient to capture the prominent wave scattering in the simulation. The Cray X1E at the Army High Performance Computing Research Center performed three of the simulations with 768 cores and  $\sim 2.67$  h wall time. The XT3 at the Engineer Research and Development Center, in the 4,096 dual-core configuration of the 2007 upgrade, performed seven simulations with 256 cores and  $\sim 6.33$  h wall time each. The saved wave-field time series contain data with  $320$  Hz Nyquist frequency and  $0.118$  m spatial sampling. We decimated the wave field by orders two and eight, respectively, for the scattering and reduced-order modeling analyses, and divided the wave-field data into sections to work within computational and memory limitations of a 16GB four-core shared-memory workstation for Fourier analysis and singular-value-decomposition processing.

## 2.2. Signal Fading Calculation

Using the sectioned wave-field data, we calculate a measure of signal fading in two steps. First we calculate mean values of the Fourier-transformed data as a function of radius from the source,  $r = \sqrt{(x - x_s)^2 + (y - y_s)^2}$ , for the aboveground wave field of each analysis, i.e.,

$$\bar{Y}_i(r, f) \equiv \text{mean} \left[ Y_i(x, y, f) \right]_{r_a \leq r < r_a + \Delta r} \quad (3)$$

$$r_a = 0, \Delta r, 2\Delta r, \dots, r_{\max}$$

where  $i = 1, 2, \dots, 9$  denotes the analysis number; and  $Y_i(x, y, f)$  is the Fourier-transformed pressure response to the broadband filtered pulse, at locations  $x, y$  and frequency  $f$ , for analysis  $i$ . The calculation of the mean at each  $r_a$  thus includes Fourier transforms from all  $x, y$  positions whose radial distance from the source are within the annular radii  $r_a$  and  $r_a + \Delta r$ . For calculations we chose  $\Delta r$  to be  $0.67$  m and excluded the wave-field data above the rooftops.

In the next step we use the values from the functions  $\bar{Y}_i(r, f)$  normalized by the corresponding radial and frequency values of the reference function  $\bar{Y}_0(r, f)$ , i.e.,

by the corresponding values from the analysis without buildings. We arrive at the measure of signal fading using the equation

$$E(\Psi(r, f)) \equiv E \left( \left| \bar{Y}_i / \bar{Y}_0 \right| \right) = \frac{1}{n} \sum_{i=1}^n \left| \bar{Y}_i / \bar{Y}_0 \right| \quad (4)$$

where  $| \cdot |$  designates complex amplitude,  $E(\cdot)$  is the expectation value, and  $n$  is the number of analyses.

## 2.3. Reduced-Order-Model Calculation

We calculate reduced-order models as a post-processing step, using frequency and impulse response relationships calculated from the Fourier-transformed input and wave-field output of the broadband FDTD models. We apply the technique by Ho and Kalman<sup>[5]</sup> for realization of state-space models, and SVD-based balanced-model truncation, as implemented in the Eigensystem Realization Algorithm (ERA)<sup>[6]</sup>. The algorithm can identify a relatively small state-space model that accurately, efficiently, and stably describes the dynamics of a multi-input multi-output system. Subsequent state-space matrix calculations can predict responses to inputs. The ERA method is applicable to propagation in linear time-invariant (LTI) systems, and thus appropriate for our acoustic computations. Previous computational research illustrated its capability for identifying state-variable models of seismic propagation phenomena<sup>[13]</sup>.

State-space equations for a discrete LTI system are:

$$x(k+1) = Ax(k) + Bu(k); \quad y(k) = Cx(k) \quad (5)$$

where  $x$  is an  $n$ -dimensional state vector;  $u$  is an  $m$ -dimensional input vector; and  $y$  is a  $p$ -dimensional output vector.  $A$  is the  $n \times n$  system matrix,  $B$  the  $n \times m$  input matrix, and  $C$  the  $p \times n$  output matrix.  $k$  is the discrete-time index. The impulse response of this system is

$$h(k) = CA^{k-1}B; \quad k = k_0 + 1, k_0 + 2, \dots \quad (6)$$

The realization or inverse problem is stated as follows: given a sequence of  $p \times m$  impulse response matrices, find a state-space model  $[ABC]$  such that Eq. (6) holds and the state-space dimension is minimal<sup>[5,6]</sup>. The first step is to assemble Hankel block-data matrices of the impulse-response data. Enabling theoretical features of ERA include the relationships between the sequence of impulse-response-data terms in the Hankel matrices, the state-space system, the reachability and observability matrices, and the application of singular-value decomposition that allows the state-space system to be derived from the data.

A Hankel matrix  $H_{J-1, J-1}$  is a block matrix formed by the product of the  $I$ -observability matrix  $V_{J-1}$  and the  $J$ -reachability matrix  $U_{J-1}$ , defined by

$$\begin{aligned}
H_{I-1,J-1} = V_{I-1} U_{J-1} &= \begin{bmatrix} C \\ CA \\ \vdots \\ CA^{I-1} \end{bmatrix}_{pI \times n} \begin{bmatrix} B & AB & \dots & A^{J-1}B \end{bmatrix}_{n \times Jm} \\
&= \begin{bmatrix} CB & CAB & \dots & CA^{J-1}B \\ CAB & CA^2B & \dots & CA^J B \\ \vdots & \vdots & \vdots & \vdots \\ CA^{I-1}B & CA^I B & \dots & CA^{I+J-2}B \end{bmatrix}_{pI \times Jm} \quad (7)
\end{aligned}$$

Equations 6 and 7 reveal that each term of the Hankel block matrix in 7 is a term of the impulse response matrix in 6, with  $k_0 = 0$ . ERA exploits this structure by an SVD operation on the Hankel matrix, and, truncating the smallest of the  $n$  singular values below a selected model order  $N$ , calculates the reduced-order model  $[ABC]_N$  using

$$\begin{aligned}
A &= \left[ \Sigma_{H_N}^{-1/2} \right] \left[ P_N^T \right] \left[ \tilde{H}_{I-1,J-1} \right] \left[ Q_N \right] \left[ \Sigma_{H_N}^{-1/2} \right]; \\
B &= \left[ \Sigma_{H_N}^{-1/2} \right] \left[ Q_N^T \right] \left[ E_{m1} \right]; \quad C = \left[ E_{p1}^T \right] \left[ P_N \right] \left[ \Sigma_{H_N}^{-1/2} \right] \quad (8)
\end{aligned}$$

where  $N$  is the number of retained singular values;  $P_N$  is the  $pI \times N$  matrix of left singular vectors;  $\Sigma_{H_N}$  is the  $N \times N$  singular value matrix;  $Q_N^T$  is the  $N \times Jm$  matrix of right singular vectors;  $E_{m1}$  and  $E_{p1}^T$  are functions of the identity matrix to isolate the input and output matrices; and  $\tilde{H}_{I-1,J-1}$  is the Hankel matrix with  $k_0 = 1$ . The corresponding eigensystem can sometimes support interpretation. In the case of wave-field data, the phase lag of the complex eigenvectors enables the inherent delays of wave propagation.

Ho and Kalman<sup>[5]</sup> proved that dimension  $n$  of a non-reduced realization, i.e., the size of  $A$ , equals the rank of the Hankel matrix.  $A$  thus has a row or column size that is a multiple of the length of the impulse-response sequence, which can be far smaller than the number of degrees-of-freedom (DOF) of a large-DOF numerical model being reduced. (This is a key feature of post-processing reduced-order modeling using high performance computing (HPC) results). Yet even with DOF and model order reductions, focus on wave-field data puts our processing in the category of large-scale system approximation<sup>[14]</sup>. The SVD computational and memory requirements are  $O(n^3)$  and  $O(n^2)$ , respectively, for a rank- $n$  full-order system<sup>[14]</sup>.

### 3. Results

Figure 4 and Figure 5 show relative power between the scattered signals and the corresponding reference signals in the aboveground wave field. These images illustrate the spatial variation of the data from which the

signal fading result derives, as well as complexity of scattering to be captured in reduced-order models. Figure 4 includes relative-power images of a single model at 90, 150, and 210 Hz. Qualitative comparison of the three results reveals similar areas and patterns of amplification and de-amplification over the frequency range. This result is of interest because it substantiates the frequency independence observed previously in signal fading measures in References 1 and 2. Figure 5 includes the remaining relative-power images for the 150 Hz frequency. These data illustrate fascinating urban sound field phenomenology, and reveal the radial and between-model statistical variations that are processed in Eq. (3) and (4), respectively.

#### 3.1. Signal Fading Curves

Signal fading as a function of range is illustrated in Figure 6. Figure 6c shows a result similar to fading curves presented in Reference 2, which have an initial downward concavity before transitioning to an exponential decay, and which are independent of frequency. The data shown in Figures 6a and 6b, for line-offsite (LOS) and non-line-of-site (NLOS) locations in the wave fields, respectively, show that the transition in the fading curves results from the increasing dominance of the NLOS data with increasing range, and that the combined LOS and NLOS data is largely independent of frequency. It is the form of the curve in 6c that we expect to statistically parameterize for sensor-placement decision support, by extending the current work to several urban terrain types, taking advantage of the frequency independence to analyze larger models, and investigating the analogy<sup>[1,2]</sup> between urban scattering with turbulent scattering.

#### 3.2. Identified State-Space Model

Figure 7 illustrates an application of a reduced-order model processed by the ERA method. The identified model had an impulse-response time series 512 samples in length (0.8-s duration). The SVD-based model truncation was principally to delete unstable noise propagation modes, leaving a wave-field model with order  $N = 460$ . Figure 7a illustrates the relative RMS error of the identified model's impulse response compared to the FDTD data. The median and mean of the relative error over the field is 7 %. Vertical strips in the error data reflect nine distinct data sections used to create, in effect, nine order- $N$  ROMs that we then reassembled into a single working model.

Figures 7b and c show snapshots of the FDTD and ROM wave fields after a Gaussian-pulse source with a 40-Hz center frequency. This pulse is different than the

Figure 2 broadband source used to create the model, and an additional FDTD analysis produced the Figure 7b result depicted. We calculated the state-space ROM response using the *lsim* function of the MATLAB Control System Toolbox<sup>[15]</sup>, running the model  $[ABC]_n$  over several minutes on a notebook computer with a 2.33 GHz Intel Core 2 Duo processor. Comparison of the Figure 7 snapshots shows that the ROM accurately reproduces the complicated scattered field of the FDTD result. Close inspection shows faint pressure ripples likely due to the ringing of the Figure 2 broadband source from the steep filter roll off. We plan to further test this technique using wave-field frequency-response results from the frequency-domain finite-element code STARS3D<sup>[16]</sup>. This application should eliminate these Gibbs-phenomenon errors, and provide an efficient means to process wave fields using high-order interpolating elements.

#### 4. Conclusion

This paper highlights our initial result from modeling urban acoustic propagation for the purpose of deriving signal fading curves for parameterization and reduced-order models that accurately capture urban sound propagation phenomena. The work applies Fourier analysis to three-dimensional urban acoustic data to generate statistical measures of signal fading and impulse-response data to identify state-space wave-field models. By these approaches we begin work to extend an existing decision support tool to urban applications, and look ahead to large-scale high-fidelity models that compute in real time or near-real time for specific urban configurations, yet have the capability to model sound propagation with phenomena such as severe multi-path scattering.

The results include signal-fading functions of distance and frequency from urban acoustic models that include structures like those in a small-city periphery. These show that the sound diminishes exponentially with distance when non-line-of-site locations become dominant in the averaged data, as is the case for turbulent scattering. In addition, the signal fading is largely independent of frequency for most of the bandwidth of the analyses.

The signal fading relationships demonstrate the ability of high-fidelity three-dimensional models to quantify scattering from urban structures. The predicted acoustic wave fields from reduced-order models, in comparison with full-model wave fields, demonstrate the potential of SVD-based model identification and reduction techniques for wave-field analysis. We conclude that the spatial processing of urban acoustic wave fields from high-performance computations

produces broadly useful measures for understanding and modeling urban wave propagation and scattering.

#### Acknowledgements

Funding support is from the Department of Defense High Performance Computing Modernization Program (HPCMP) Software Applications Institute I-01: Institute for Maneuverability and Terrain Physics Simulation; USAERDC 6.2 Program "URBAN Seismic/Acoustic Signatures and Phenomenology" and ILIR Program "Reduced-Order High-Fidelity Models for Signature Propagation." Computational support is from HPCMP Challenge Project C2X, "Decision Support for Seismic and Acoustic Sensors in Urban Terrain".

#### References

1. Wilson, D.K., R. Bey-Hernandez, and V.E. Ostashev, "Statistical Models for Fading and Coherence of Sound in Urban Environments." *J. Acoust. Soc. Am.*, Vol.120, No.5, Pt.2, pp. 3336-3337, 2006.
2. Wilson, D.K., R. Bey-Hernandez, and V.E. Ostashev, "Statistical Characterization of Sound-Wave Scattering in Urban Environments." *Proc.12<sup>th</sup> Long-Range Sound Propagation Symposium*, New Orleans, LA, October 2006.
3. Wilson, D.K., "Sensor Performance Evaluator for Battlefield Environments (SPEBE) Tutorial." *US Army ERDC-CRREL Technical Report TR-06-12*, 2006.
4. Lucia, D.J., P.S. Beran, and W.A. Silva, "Reduced-Order Modeling: New Approaches for Computational Physics." *Prog. in Aerospace Sci.*, 40, pp. 51-117, 2004.
5. Ho B.L. and R.E. Kalman, "Effective Construction of Linear State-Variable Models from Input/Output Functions." *Regelungstechnik*, 14, pp. 545-548, 1966.
6. Juang, J.N., *Applied System Identification*, Upper Saddle River, NJ, Prentice Hall, 1994.
7. Wilson, D.K., and L. Liu, "Finite-Difference, Time-Domain Simulation of Sound Propagation in a Dynamic Atmosphere." *US Army ERDC-CRREL Technical Report TR-04-12*, 2004.
8. Cudney, H.H., S.A. Ketcham, and M.W. Parker, "Verification and Validation of Acoustic Propagation Over Natural and Synthetic Terrain." Submitted, Proc.2007 Users Group Conference, DoD High Performance Computing Modernization Program, 2007.
9. Ketcham, S.A., J. Lacombe, T.S. Anderson, and M.L. Moran, "Seismic Propagation from Humans in Open and Urban Terrain." *Proc.2005 Users Group Conference, DoD High Performance Computing Modernization Program*, IEEE Computer Society, pp. 270-277, 2005.
10. Cerjan, C., R. Kosloff, and M. Reshef, "A Nonreflecting Boundary Condition for Discrete Acoustic-Wave and Elastic-Wave Equations." *Geophys.*, SEG, Vol. 50, pp.705-708, 1985.
11. Parker, M.W., S.A. Ketcham, and H.H. Cudney, "Acoustic Wave Propagation in Urban Environments." Submitted,

Proc.2007 Users Group Conference, DoD High Performance Computing Modernization Program, 2007.

12. Fordyce, D.F., "Standardized Urban Terrain Templates Based on UTZs." Presentation at 71<sup>st</sup> MORS Symposium, Military Operations Research Society, Quantico, VA, 2003.

13. Ketcham, S.A., M.L. Moran, J. Lacombe, R.J. Greenfield, and T.S. Anderson, "Seismic source model for moving vehicles." *Trans. Geosc. Rem. Sens.*, IEEE 43, pp.248–256, 2005.

14. Antoulas, A.C., *Approximation of Large-Scale Dynamical Systems*, SIAM, Philadelphia, PA, 2005.

15. The Mathworks, Control System Toolbox 8, User's Guide, The Mathworks, Inc., Natick, MA, 2007.

16. Dey, S. and D.K. Datta, "A Parallel hp-FEM Infrastructure for Three-Dimensional Structural Acoustics." *Int. J. Num. Meth. Eng.*, Vol. 68, 206, pp.583–603.

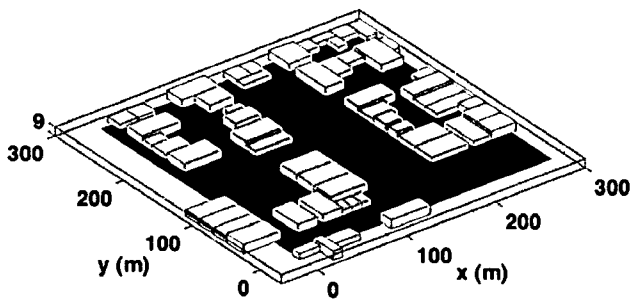


Figure 1. Isometric view of propagation model SCP02 derived from small-city-periphery urban template. The black surface spans the ground-level extents of the model. The grey blocks are two and three story buildings that are contained wholly or partially within the extents.

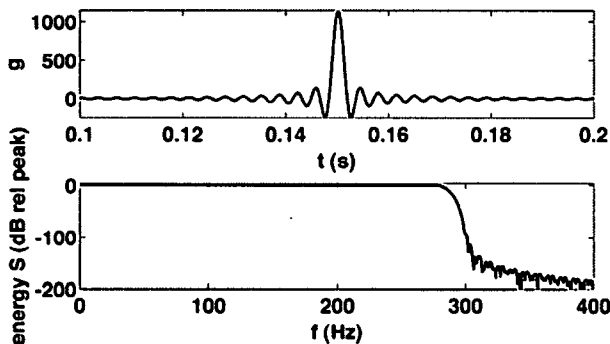


Figure 2. (a) Time series  $g$  and (b) energy spectrum  $S$  of filtered-pulse dilatation-rate source. The time series shows ringing that results from applying a steep low-pass filter to the pulse. The energy spectrum reflects the filter in its roll off starting below 300 Hz.

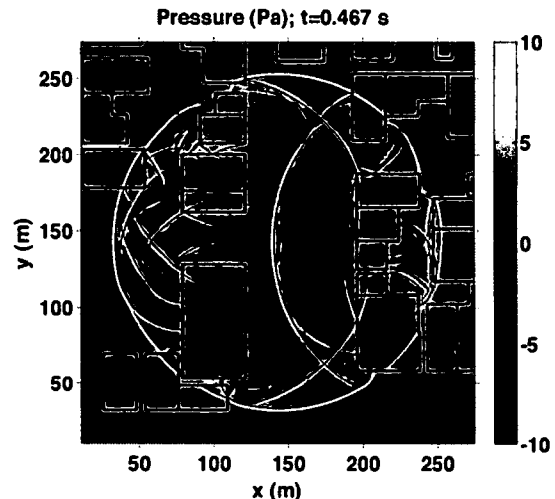


Figure 3. Snapshot at simulation time=0.467 s of pressure from broadband source, just above ground-and-rooftop surface of the SCP02 model. The pressure scale is truncated at 5% of maximum amplitude to highlight the dominant and reflected wave arrivals.

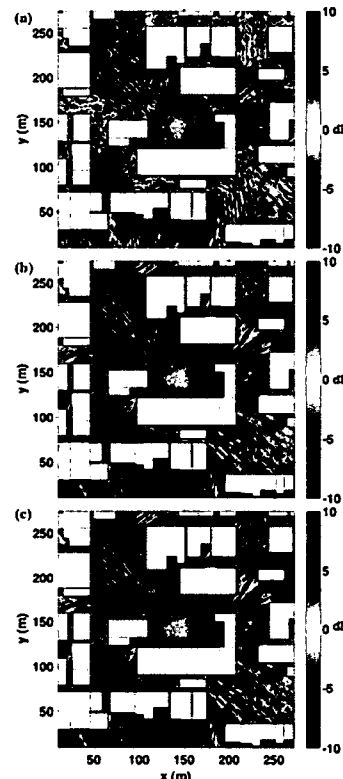


Figure 4. Comparison of relative power in just-aboveground wave field at propagation frequencies (a) 90 Hz, (b) 150 Hz, and (c) 210 Hz, respectively, in model SCP04. The relative power in dB was calculated using  $20 \log_{10} (|Y_s(x, y, f) / Y_o(x, y, f)|)$ . The images are green in areas of constructive multi-path interference, and red in areas of destructive multi-path interference. The white stars indicate x-y location of source. The white areas are rooftops.

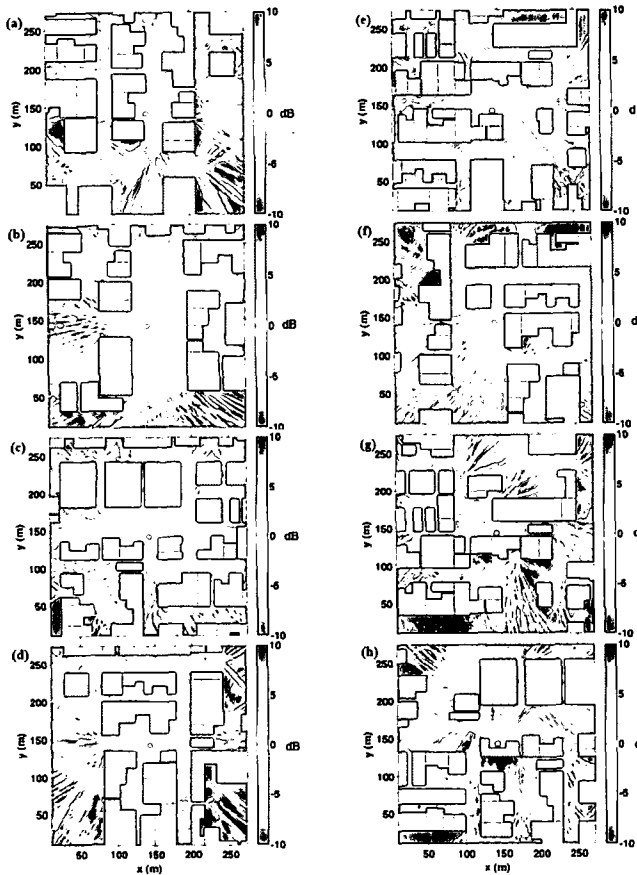


Figure 5. Comparison of relative power at 150 Hz propagation frequency from eight additional models, (a) SCP01, (b) SCP02, (c) SCP03, (d) SCP05, (e) SCP06, (f) SCP07, (g) SCP08, and (h) SCP09.

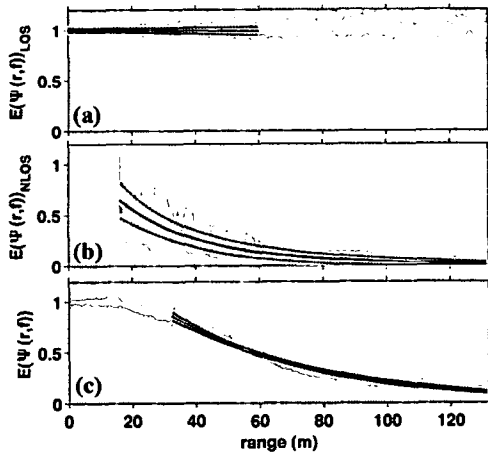


Figure 6. Measures of signal fading using Equation 4 for the nine analyses, relative to the no-building analysis. (a) Line-of-site data. (b) Non-line-of-site data. (c) Combined LOS and NLOS data. The gray lines are calculated expected values from the discrete frequencies 50, 60, 70, ... 240 Hz. The darker solid lines are exponential fits to the data in each case, and the dashed lines are at  $\pm$  one standard deviation.

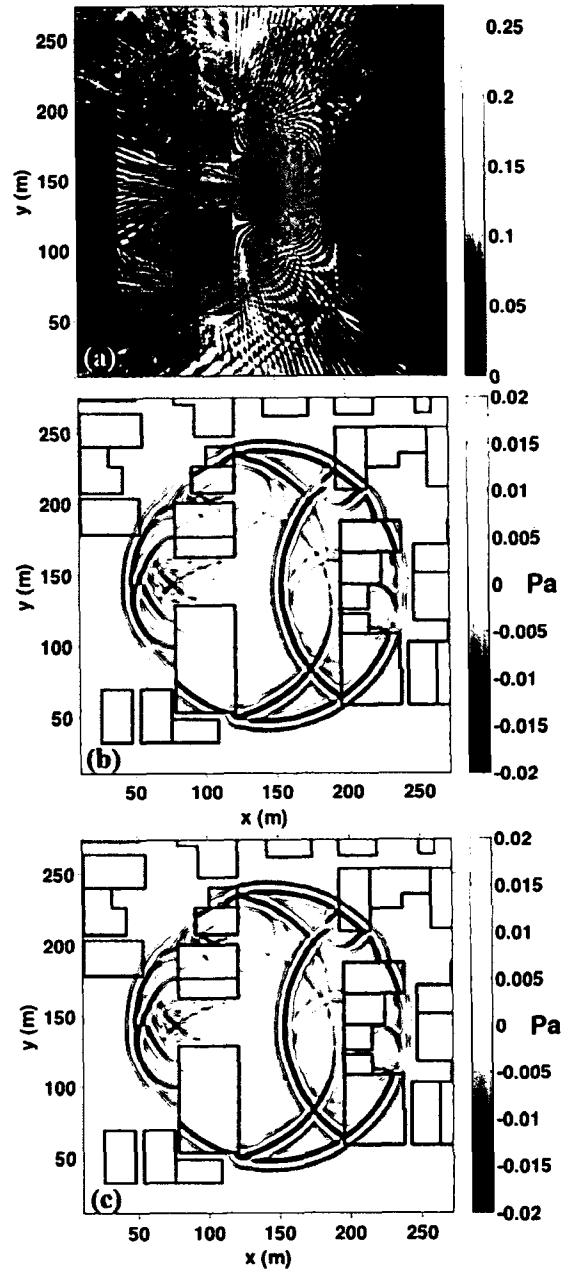


Figure 7. Results of state-space model identification, model SCP02. (a) Relative RMS error between FDTD and ROM wave-field impulse responses. (b) Snapshot at  $t=0.317$  s of FDTD sound pressure from Gaussian-pulse dilatation-rate source. (c) Corresponding ROM snapshot.